Preliminary Characterization of the Irradiation Facilities Within the LEU-Fueled UMass-Lowell Research Reactor

John R. White, Areeya Jirapongmed, and Justin Byard

Chemical and Nuclear Engineering Department

University of Massachusetts Lowell

Lowell, MA 01854

PHYSOR 2000

Pittsburgh, PA

May 7-11, 2000

PRELIMINARY CHARACTERIZATION OF THE IRRADIATION FACILITIES WITHIN THE LEU-FUELED UMASS-LOWELL RESEARCH REACTOR

John R. White, Areeya Jirapongmed, and Justin Byard

Chemical and Nuclear Engineering Department
University of Massachusetts Lowell
Lowell, MA 01854

John_White@uml.edu Areeya_Jirapongmed@student.uml.edu Justin_Byard@student.uml.edu

ABSTRACT

The University of Massachusetts Lowell owns and operates a 1 MW swimming pool reactor that is currently loaded with high enriched uranium (HEU) fuel. However, conversion to low enriched uranium (LEU) fuel is planned for the summer of 2000. The new LEU core has a substantially smaller footprint and a new fuel assembly design. Thus, the new configuration represents a significant change relative to the current configuration, which will have some affect on operations and use of the experimental facilities. In preparation for the actual conversion, a series of analyses have been completed to evaluate the overall performance of the new core and its affect on current operations. The current study, in particular, focussed on characterization of the irradiation facilities in the new LEU-fueled core. This paper briefly summarizes the models and methods used to estimate the neutron and gamma environments that are expected in these facilities. It also provides a wealth of actual data that can be used to support the continued use of the experimental facilities within the new LEU core configuration.

INTRODUCTION

Conversion from high enriched uranium fuel to low enriched uranium (LEU) fuel at the 1 MW UMass-Lowell Research Reactor (UMLRR) is currently planned for summer 2000. A new 21-element LEU core configuration containing 19 full fuel elements and 2 partial elements has recently been designed,[1] and a layout of the new core is sketched in Fig.1. This configuration supports a variety of traditional experimental facilities including six beam ports and a large graphite thermal column on the core periphery, and several radiation basket assemblies within the 9x7 grid arrangement. The new LEU core also highlights a central flux trap facility where large increases in the fast and thermal fluxes relative to the other facilities are expected. In preparation for actual conversion to the LEU core, a series of studies have been initiated to fully characterize the behavior of the new core. The purpose of the current study was to predict the

neutron and gamma flux distributions throughout the new core, and to quantify the expected radiation environment within the primary irradiation facilities. This work has now been completed and the goal of this paper is to overview the methods and models used in the calculations and to highlight the key results of this study. The data generated in this work should assist in the daily operation of the UMLRR as well as provide support for the design and analysis of the various experimental programs that use its irradiation facilities.

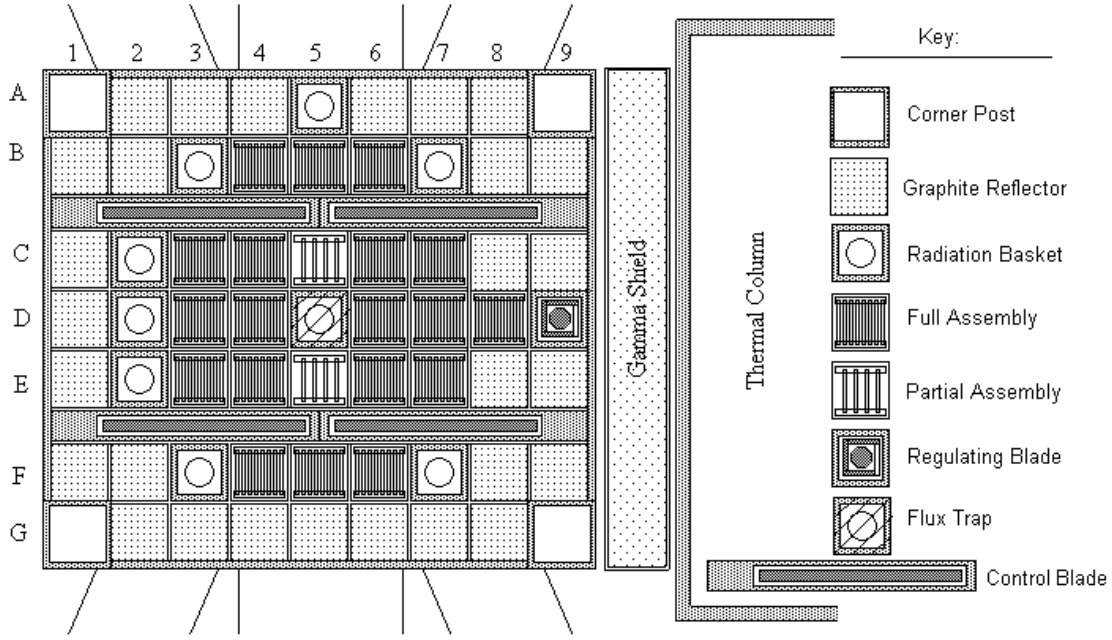

Fig. 1 Reference LEU core configuration for the UMLRR.

COMPUTATIONAL METHODOLOGY

Computer modeling always involves some approximation to the real physical system and our knowledge of the underlying physical processes that are present. As part of a larger study to develop a wide range of modeling capabilities for the new LEU core, we have compared diffusion theory versus transport theory using the VENTURE[2] and DORT[3] codes, 2-D geometry versus 3-D geometry, a buckling versus no-buckling approximation, few-group theory versus multigroup theory, and, to some extent, deterministic modeling in VENTURE and DORT versus stochastic modeling with a preliminary MCNP model.[4] Most of these in-house evaluations are unpublished, but some comparisons and some further descriptions of the computational models are given in Refs. 1 and 5. There are certainly pros and cons to each method and, of course, the numerical results certainly vary among the different approximations. However, the various models are all generally self-consistent and they show the same general features and behavior.

Although several computational options are available, an estimate of the neutron and gamma radiation environment throughout the system is generally obtained from a 2-D XY DORT computation. Our traditional approach for modeling with DORT is to restrict most analyses to

be of the fixed-source type, rather than an eigenvalue k_{eff} problem. This is the suggested mode of operation because transport theory analyses in DORT are generally much more computationally intensive compared to diffusion theory calculations in VENTURE. However, for fixed-source computations with no upscatter, only one outer iteration is required within the code solution algorithm. Since this represents a significant improvement in runtime relative to eigenvalue or fixed-source problems with upscatter (i.e. problems requiring multiple outer iterations), this mode of operation is definitely the preferred DORT solution scheme. However, since the core physics problem is really an eigenvalue problem, the overall problem solution becomes a two-phase process -- we first compute the fission source using diffusion theory, and then this distributed source is used to drive a fixed-source transport problem.

In equation form, we can represent the core physics problem as an eigenvalue problem of the form

$$(L - \lambda F)\phi = 0 \tag{1}$$

where $L\phi$ accounts for the loss and scattering components of the particle balance equation and $F\phi$ represents the fission source term. The eigenvalue, λ, is simply the inverse of the multiplication factor $(\lambda = 1/k_{eff})$.

If the fission source term is moved to the right hand side of eqn. (1), then the balance equation can be written as

$$L\phi = \lambda F\phi = Q \tag{2}$$

For known Q, this expression becomes a fixed-source problem.

The VENTURE code is used to solve eqn. (1) using a few-group diffusion theory approximation. Near the fueled core region, diffusion theory is usually adequate and it gives a good estimate of the eigenvalue and the power distribution within the fueled regions. The neutron source distribution needed for use with eqn. (2) is simply related to the power distribution, as described below.

First let's denote $PD(\vec{r})$ as the power density distribution, where

$$PD(\vec{r}) = \kappa \sum_{g'} \Sigma_{fg'}(\vec{r})\phi_{g'}(\vec{r}) \tag{3}$$

and the symbols have their traditional meaning. κ gives the average energy release per fission. Now, the multigroup fission source, $Q_g(\vec{r})$, is given by

$$Q_g(\vec{r}) = \lambda \chi_g \sum_{g'} \nu\Sigma_{fg'}(\vec{r})\phi_{g'}(\vec{r}) \tag{4}$$

Combining eqns. (3) and (4) gives

$$Q_g(\vec{r}) = \alpha \chi_g PD(\vec{r}) \tag{5}$$

where the power-to-source conversion factor, α, is given by

$$\alpha = \lambda\nu/\kappa \tag{6}$$

For an eigenvalue near unity, $\nu \approx 2.43$ neutrons per fission, and $\kappa \approx 200$ MeV per fission, the conversion factor becomes $\alpha \approx 7.6 \times 10^{10}$ neutrons/cm^3-sec per watt/cm^3.

Thus, the overall strategy for performing the space-energy flux calculations in DORT involves a four-step process:

1. Perform VENTURE few-group diffusion theory calculations for the desired configuration to determine the power density distribution, $PD(\vec{r})$.

2. Using eqns. (5) and (6), generate the source density distribution, $Q_g(\vec{r})$, for use in DORT.

3. Perform DORT multigroup fixed-source transport calculations to determine the space and energy dependent flux distribution, $\phi_g(\vec{r})$, for the configuration of interest.

4. Process the large amount of data from DORT into useable form (i.e. determine fast, epithermal, and thermal fluxes for plotting purposes, perform reaction rate integrals as needed, compute neutron and gamma energy deposition rates, etc.).

Several small problem-dependent Matlab and Fortran codes have been written over the last year or so to assist in the manipulations involved in Steps 2 and 4. In particular, a code called Plot_Vpwd was written to assist in the Step 2 manipulations, and the in-house PROCESS and Plot_Flux codes are used to evaluate the DORT (and VENTURE) output files. The Plot_Vpwd code plots the VENTURE power distribution and, on option, writes a significant portion of the DORT input file, including the spatial distribution of the fixed source. The code is broken into two main components. The first part of Plot_Vpwd reads the binary power density file from a VENTURE run and plots the 1-D power distribution profiles through the peak power location. It can also plot 2-D power density surface profiles in any XY, XZ, or YZ plane of interest. The second part is only executed for a 2-D XY model and, if desired, it automatically generates the geometry information (2**, 4**, and 8$$ arrays), material distribution (9$$ array), and the spatial part of the distributed source (96** array) needed for a DORT calculation. The 2-D DORT model, on option, can also include a simple DB^2 transverse leakage approximation (6** array) with the same fixed buckling as used in the VENTURE model. This automation of a large portion of the DORT input file has significantly enhanced our ability to perform multigroup coupled neutron-gamma computations for the LEU-fueled UMLRR. This semi-automated DORT input preparation is only available, however, if a VENTURE XY model has been previously developed.

The PROCESS and Plot_Flux output processing codes are also invaluable in working with the VENTURE and DORT results. PROCESS allows one to extract 1-D flux or reaction rate profiles from DORT in the x or y direction at any user-specified location (referred to as I-profiles and J-profiles, respectively). It can also generate energy-dependent flux and reaction rate information averaged over any zone of interest (referred to as E-profiles). In addition, the Plot_Flux routine can plot a variety of 1-D curves or 2-D surface maps using the VENTURE- or DORT-generated scalar flux files. Many of the subsequent results presented here were generated with these auxiliary routines.*

* Another processing code, called Plot_Vgeo, produces a color-coded zone/material map for the given computational model and automatically generates large portions of the VENTURE input file from a standard spreadsheet description of the geometric model (see Ref. 5 for more details).

Consistent sets of DORT and VENTURE cross sections were developed specifically for the LEU core using several modules of the SCALE system[6] and the base VITAMIN-B6 library.[7] The original 199/42-group energy structure in VITAMIN-B6 was collapsed to 47 neutron groups and to 20 gamma groups for the DORT calculations and to a simple 2-group neutron library for use in the VENTURE eigenvalue calculations. The coupled 67-group DORT library is fully compatible with the energy structure from the BUGLE-96 library[8] and many of the response functions from the BUGLE-96 distribution were used as part of our overall analysis. The reader is referred to Ref. 5 for further details on the cross-section generation procedure.

Finally, it should be noted that, in all the subsequent results reported here, the 2-D flux values from the DORT calculations for operation at 1 MW have been multiplied by an axial peaking factor of 1.4. This was done to roughly approximate the fluxes that might be expected in the peak axial plane where many experimental irradiations are made. This is only a rough estimate because the axial flux profile varies with energy and radial location. An axial peaking factor of 1.4 is appropriate for the thermal fluxes near the center of the core (obtained from a 3-D VENTURE model[5]). However, this is probably a high estimate, for example, for the axial gamma distribution on the core periphery. Lacking 3-D space-energy information from a 3-D transport code, a single constant peaking factor is usually applied to the 2-D XY results.

In closing this section, we can summarize the base 2-D XY model development with a few pictures that show the zone and material maps used and the final VENTURE power density distribution that was computed. The reference XY model is referred to locally as the LEU215 core configuration. This model is identical in VENTURE and DORT and it contains nearly 190 zones within a 175x170 mesh grid. A color-coded zone/material map for the entire 2-D model is shown in Fig. 2. Each of the 34 possible homogeneous material compositions is identified on the right side of the figure, and its associated color is mapped to the appropriate core locations where this material is present. An expanded view of this same picture is given in Fig. 3, so that some of the as-modeled details of the core region can be more easily identified. Note that these figures show the actual modeled geometry and they try to approximate the real heterogeneous geometry that is idealized in the geometry sketch of Fig. 1 (i.e. Fig. 1 is only a rough sketch that illustrates some of the heterogeneous detail that is present in the real system).

The link between the VENTURE and DORT models is the VENTURE-generated power distribution. This information is converted into a distributed source for use in DORT within the Plot_Vpwd code. A qualitative view of the computed VENTURE power density is shown in Fig. 4. When this is multiplied by the fission spectrum and a power-to-source normalization factor (see above), the power density distribution, $PD(\vec{r})$, becomes the distributed source, $Q_g(\vec{r})$, for DORT. The spatial structure observed here is consistent with expectations, with zero power in the non-fueled regions and with peak power densities in the fueled regions near the water gaps and the water-filled flux trap, radiation baskets, and control blade channels. This information represents that last item needed to complete the DORT input. Thus, we are now ready to look at the actual DORT results and the characterization of the experimental facilities in the LEU fueled UMLRR.

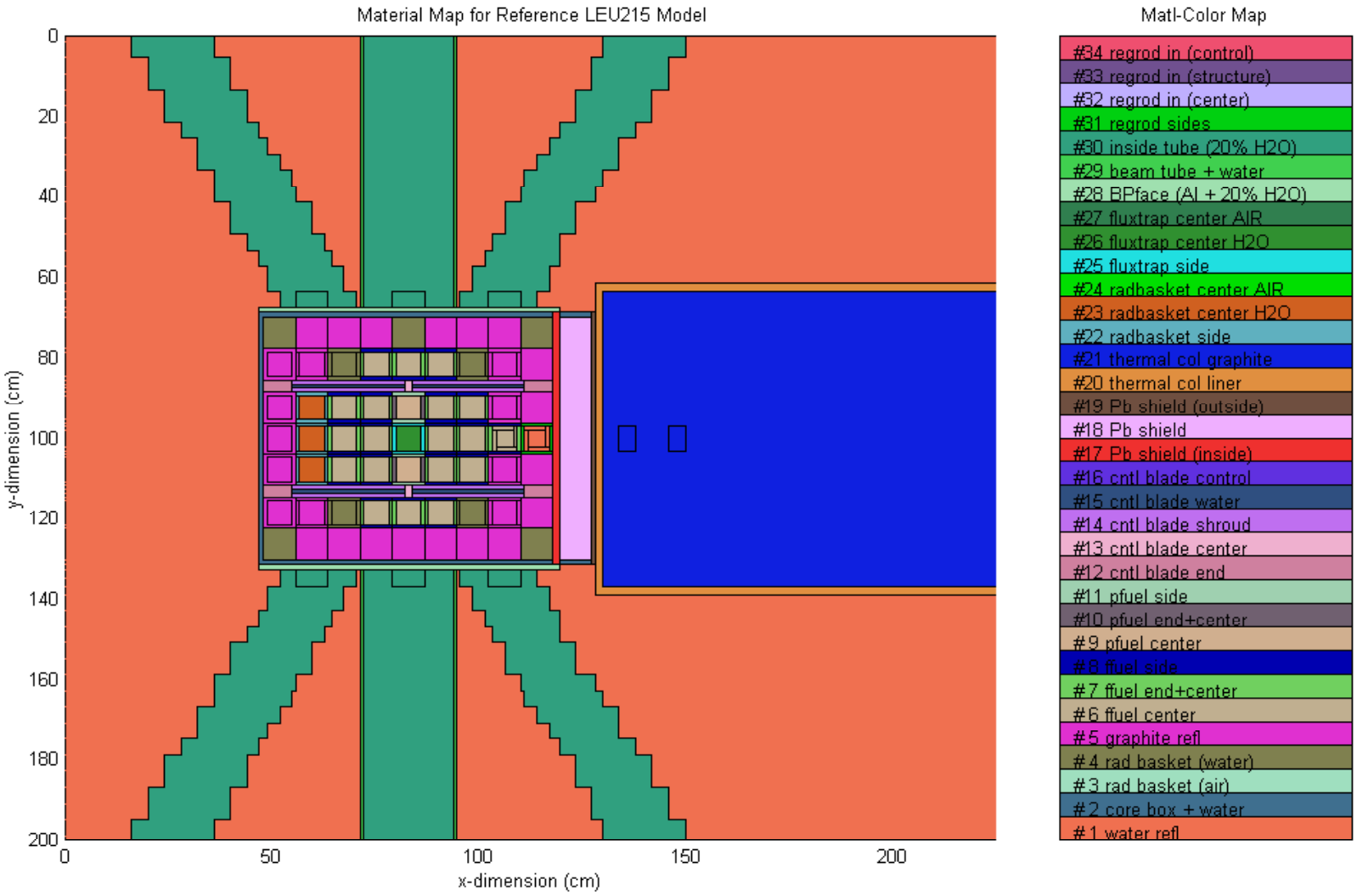

Fig. 2 Material/zone map for the reference UMLRR LEU 2-D XY calculational model.

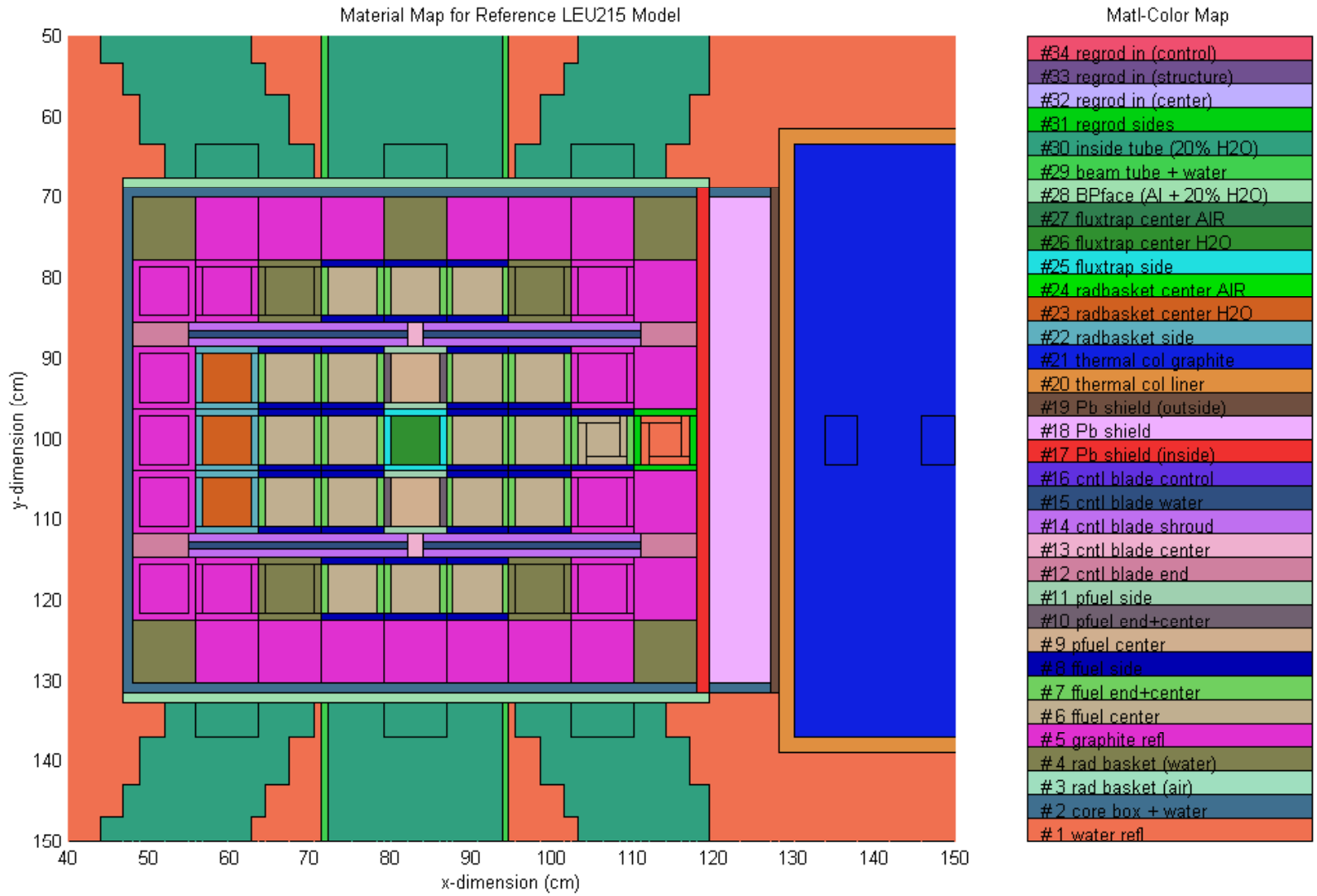

Fig. 3 Expanded view of the core region for the reference UMLRR LEU 2-D XY calculational model.

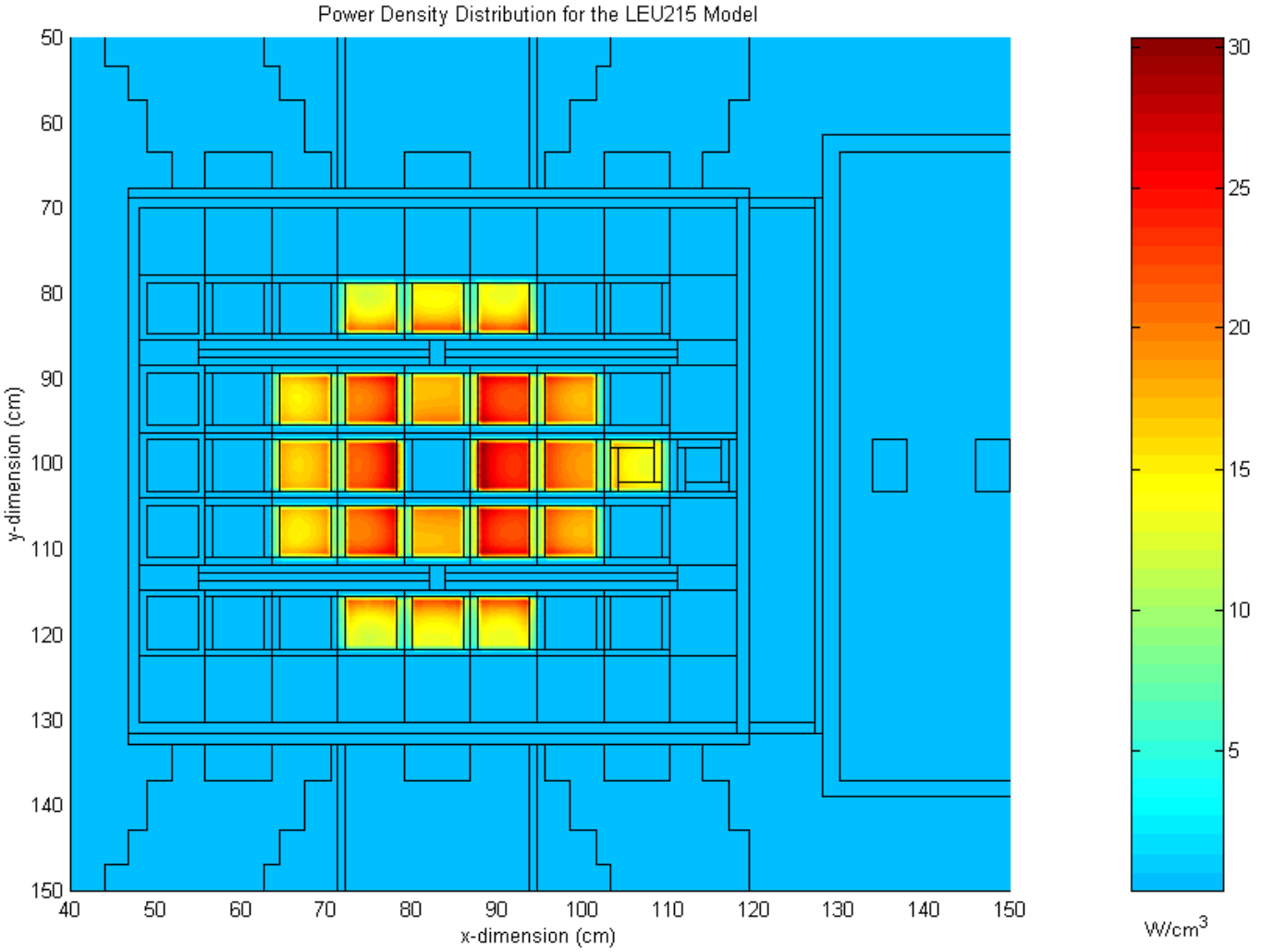

Fig. 4 VENTURE-generated power density distribution for the reference LEU XY core model.

CHARACTERIZATION OF THE EXPERIMENTAL FACILITIES

The DORT calculations focused on the characterization of the experimental facilities within the LEU-fueled UMLRR, including the central flux trap, the radiation baskets on the left core boundary, the six beam ports, and the large thermal column on the right side of the reactor -- see Figs. 1-3 for proper orientation. A series of zones were defined within the models for edit purposes, and lots of summary integral information has been accumulated for these regions. In addition, various space- and energy-dependent 1-D flux profiles and 2-D surface distribution plots were generated that give a good qualitative picture of the overall neutron and gamma flux distributions throughout the system. Summary data from these computations are presented in this section.

XY Spatial Distributions (2-D Color Contour Plots)

To illustrate the typical spatial distribution of the fluxes in the reference LEU core configuration, the DORT 67-group information was integrated over energy to give four broad-group fluxes (three neutron groups and one gamma group). For the neutron data, the fast group includes neutrons above 0.1 MeV, the thermal group covers energies below 1.0 eV, and the epithermal group includes all energies between these limits. The single gamma group represents an integral over all 20 gamma groups within the base 67-group library structure.

Several qualitative plots that present a big-picture view of the expected radiation environment within the LEU-fueled UMLRR are given in Figs. 5-9. The first two figures focus on the fast and thermal flux distributions in the core region. The flux magnitude is represented by a color map that is scaled to a linear grid. This allows some of the more important details to be seen in these XY spatial distributions. For example, Fig. 5 shows a slight dip in the fast flux in the central flux trap and a slight skew in the overall distribution towards the right side of the core. Similarly, some details in the thermal flux distribution can also be seen in Fig. 6, with the largest peak occurring in the flux trap region and several local peaks in the water-filled control blade locations and in the radiation baskets that surround the fueled central core.

Figures 7-9 show the same information, but on a more global scale. The flux magnitude is again represented by a color map, but this time it is scaled to a logarithmic grid. This allows a better view of the radiation environment throughout the whole system -- at least in a qualitative sense. For example, it is easy to see the affect of the beam ports on the fast and thermal fluxes in Figs. 7 and 8. Also, Fig. 9 clearly shows the effectiveness of the gamma shield on the right side of the UMLRR core. It is also apparent from these global representations that gamma attenuation in water is significantly different than neutron attenuation, since the gamma flux is still on the order of 10^{12} gammas/cm^2-s well into the water reflector and beam port regions. The neutron fluxes, on the other hand, have decreased by 3-4 orders of magnitude over the same range.

These qualitative flux distributions are quite informative since they paint a general picture that is easy to understand within the context of basic theory. As such, they can be quite useful as an educational tool for the operations staff and as a good visual aid in introductory courses on nuclear theory. They are, however, not particularly well suited for detailed quantitative analyses.

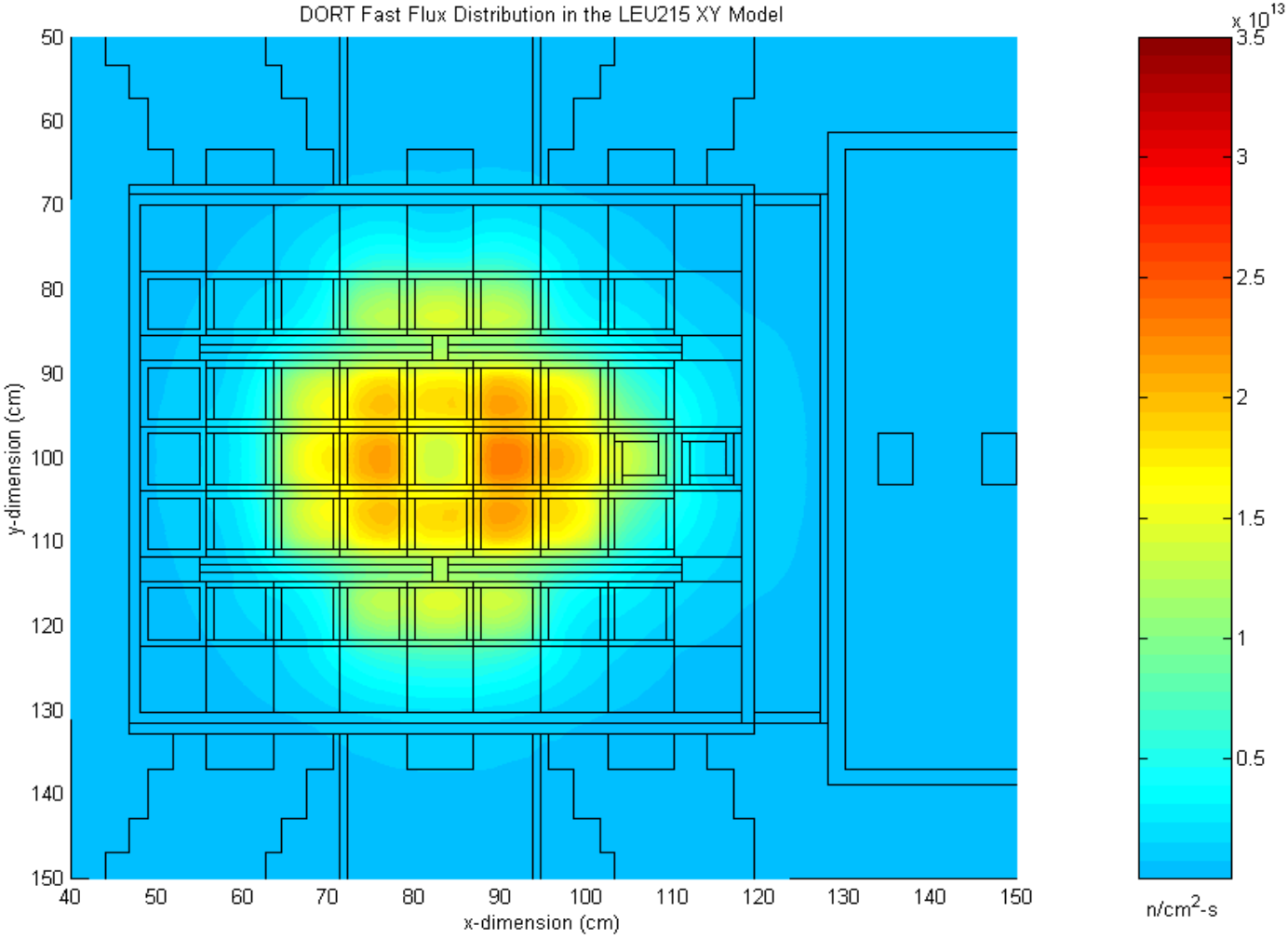

Fig. 5 Expanded view of the expected fast flux distribution in the LEU-fueled UMLRR core.

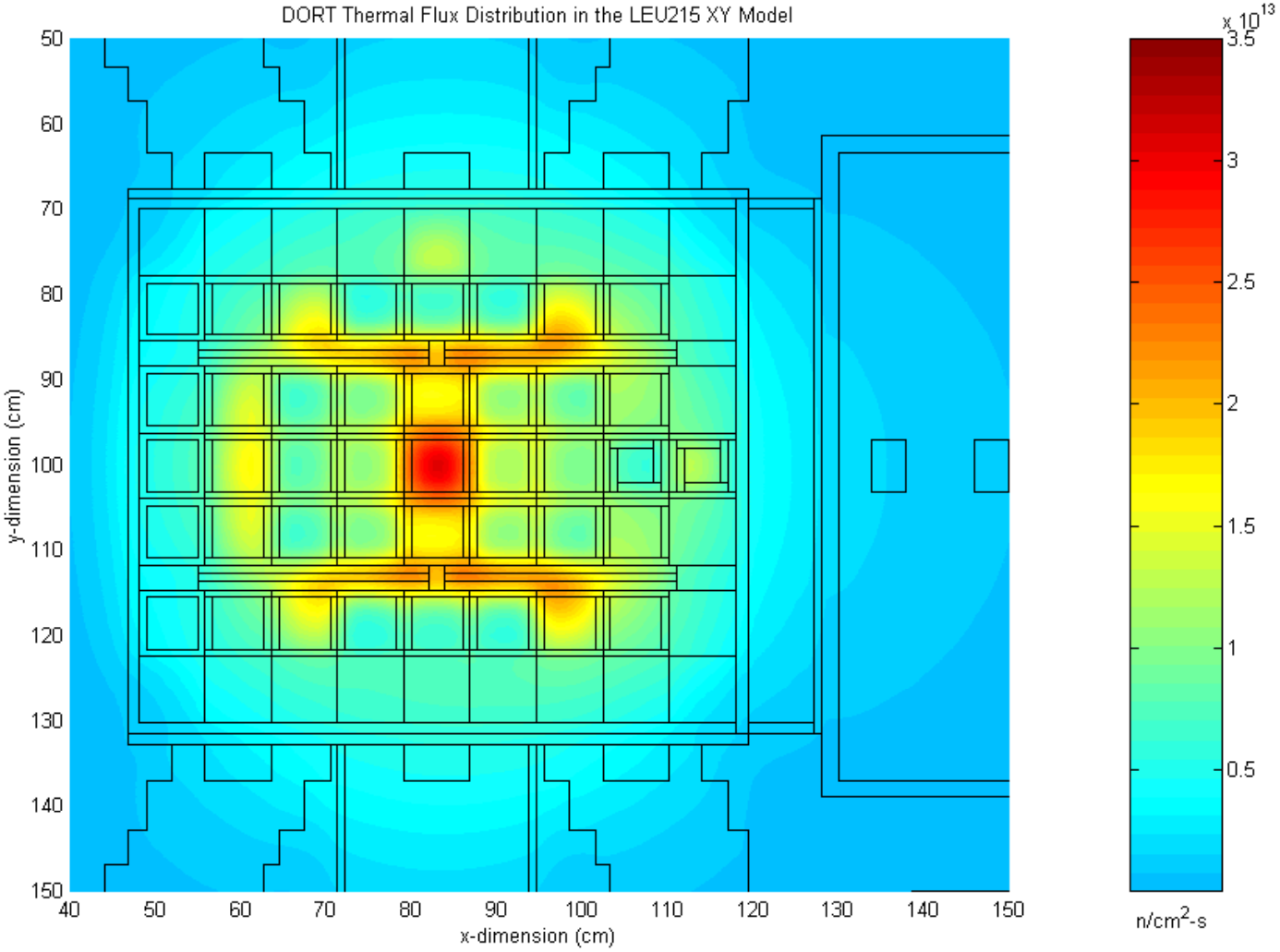

Fig. 6 Expanded view of the expected thermal flux distribution in the LEU-fueled UMLRR core.

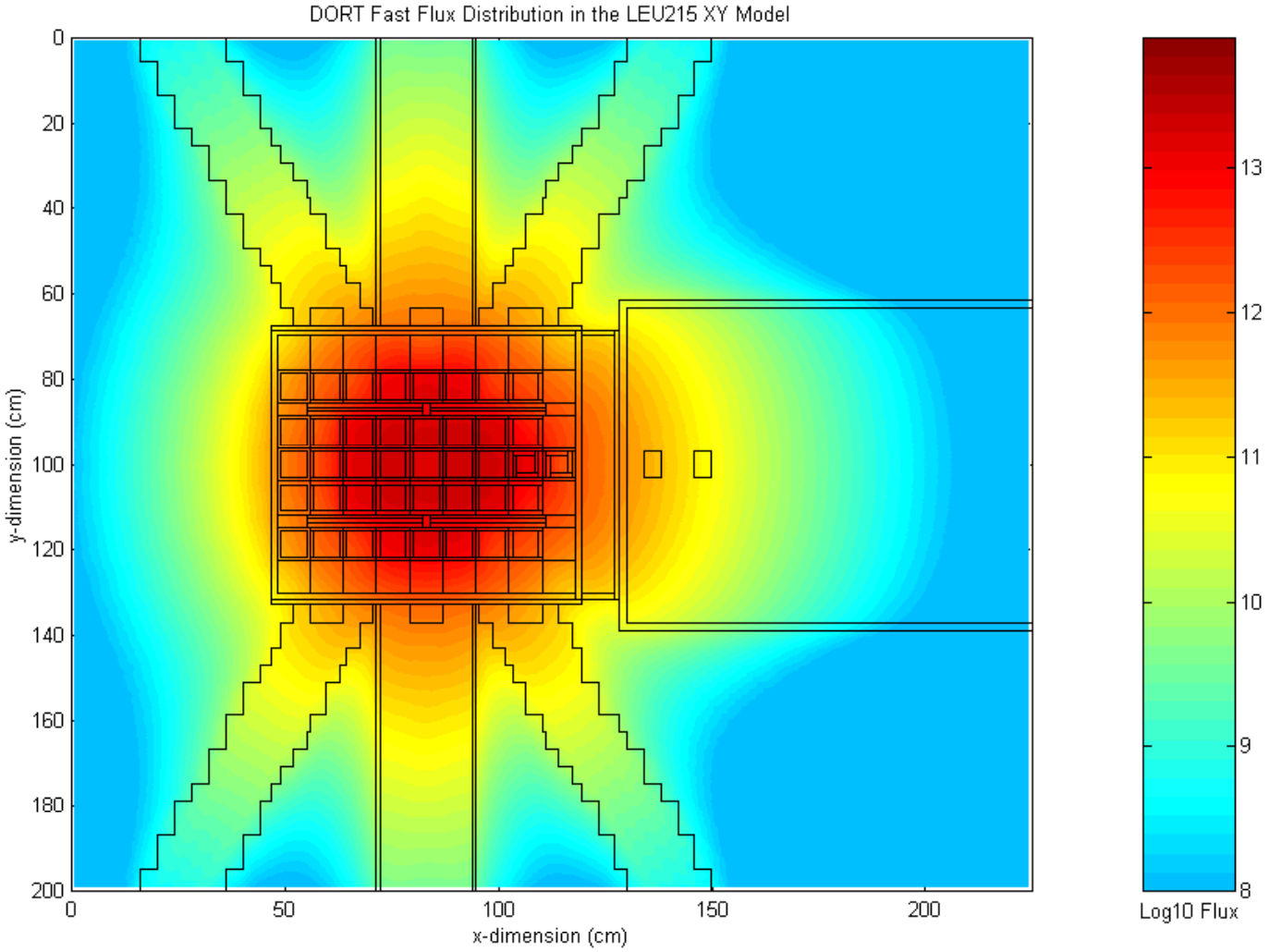

Fig. 7 Global view of the expected fast flux distribution in the LEU-fueled UMLRR (log scale).

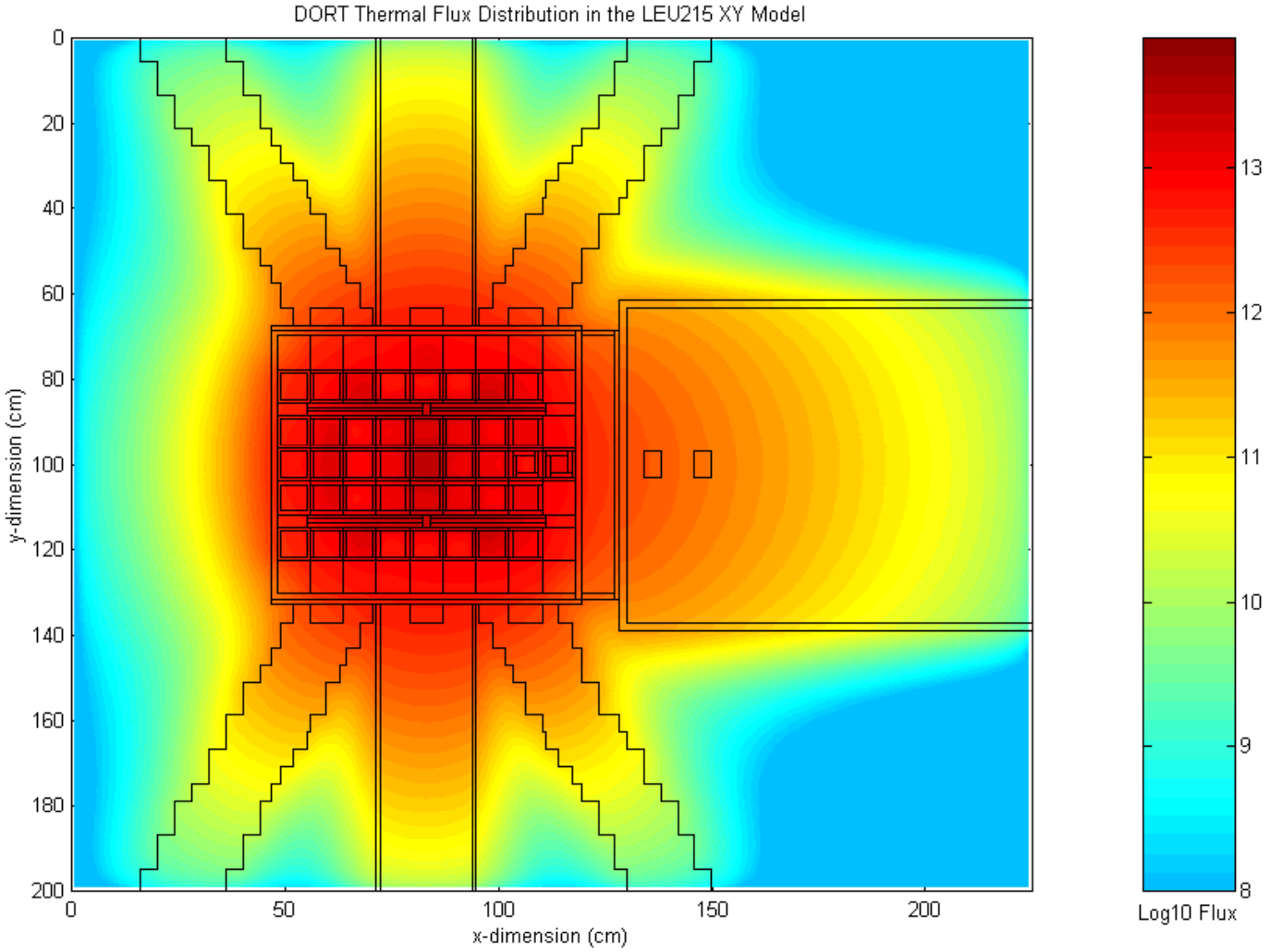

Fig. 8 Global view of the expected thermal flux distribution in the LEU-fueled UMLRR (log scale).

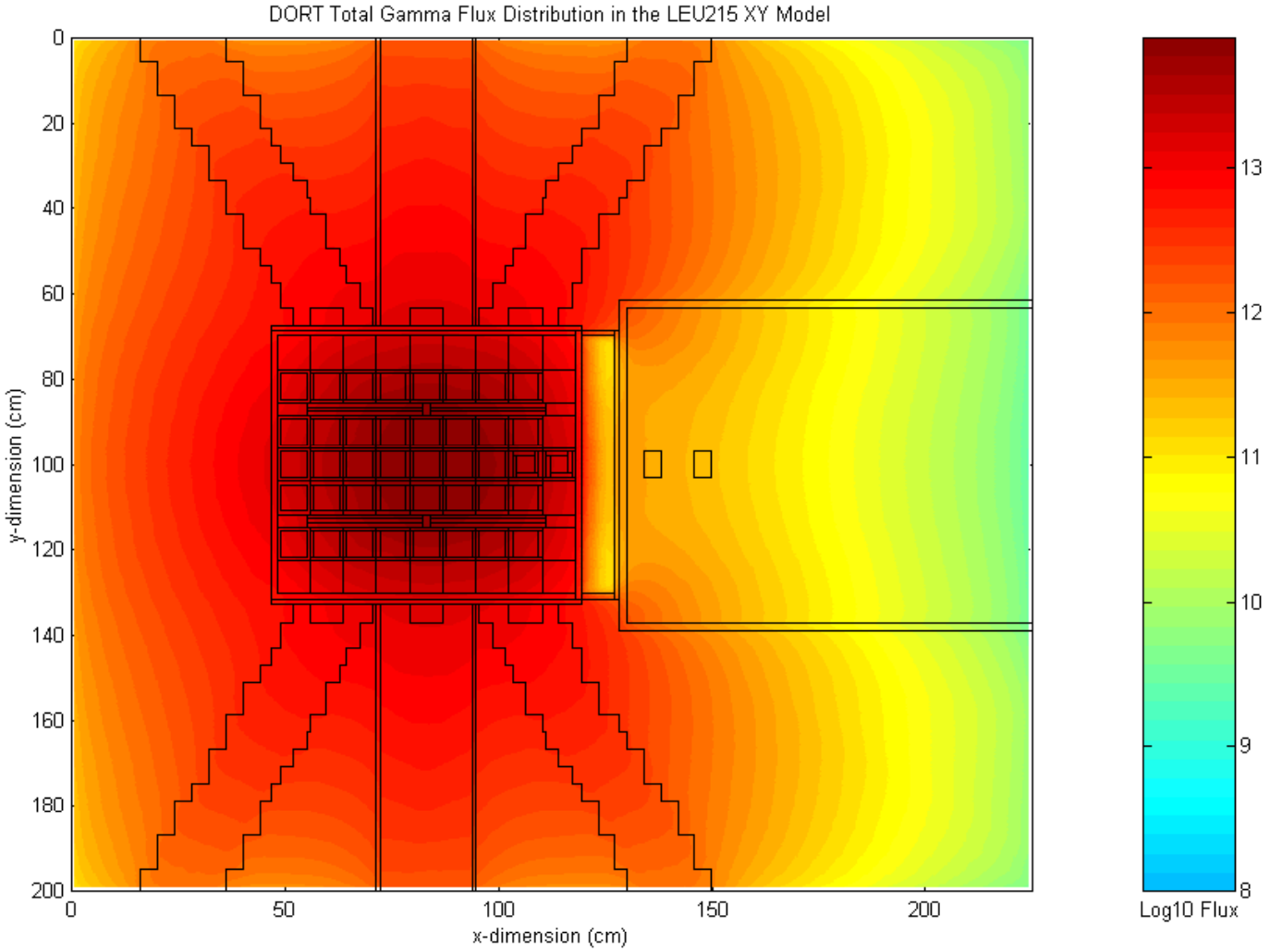

Fig. 9 Global view of the expected total gamma flux distribution in the LEU-fueled UMLRR (log scale).

X-Direction Spatial Distributions (I-profiles)

A more quantitative representation of the radiation environment within the reactor can be obtained from various 1-D profiles in the vicinity of a particular irradiation facility of interest. For example, the broad-group fluxes that were collapsed from the base 67-group information can be plotted along any X-directed radial line or Y-directed axial line of interest. An E-profile, which shows the energy spectrum for a specific zone in the computational model can also be easily generated. These 1-D profiles can give more quantitative information that the XY spatial profiles given above.

In particular, for a Y location that passes through the center of the core, the broad-group fluxes were plotted versus the X variable in Fig. 10. Note that a linear scale is used for the top plot for the fast, epithermal, and thermal neutron fluxes, and a log scale is used in the lower curves that show the X-directed spatial profiles for the total neutron flux and the total gamma flux. In general, the X-directed spatial distributions generally follow expected behavior, as follows:

- Large thermal peaks are apparent in the radiation basket on the left side, in the central flux trap, and in the regulating blade location with the blade in its control-out configuration.
- Three minor thermal peaks can also be seen and these coincide with the edges of the fuel assemblies where additional thermalization occurs. This extra thermalization occurs because of the dummy aluminum plates and associated water gap on each edge of the assembly (note that the LEU fuel element has 16 central fuel plates and 2 end aluminum plates).[5]
- We can see that the fast flux tends to dip where the thermal flux peaks, but the minima in the fast profiles generally have smoother transitions because of the longer mean free path associated with the higher energy neutrons.
- Just outside the core, we see a more rapid decrease in the fast and epithermal fluxes relative to the thermal flux because of the large regions of water or graphite in the system (and these materials are very good moderators).
- Also apparent is the significant attenuation of the gamma flux in the lead shield. This was expected, and it simply shows that the shield is performing as designed.

Y-Direction Spatial Distributions (J-profiles)

A similar set of spatial flux profiles was also generated versus the Y variable along the core centerline in the X direction, and these are displayed in Fig. 11. This Y-directed cut passes through the central beam ports (at the ends) and directly through the flux trap in the center of the core. Again, everything seen here is as expected. For example, the thermal flux peak in the center is the result of the flux trap and the twin peaks on either side of center occur because of the thermalization of the fast neutrons within the water-filled control channels. The large broader thermal peak just inside the core box on the left is due to the source holder that occupies the A5 grid position. A similar discussion for the fast flux easily explains the oscillation-like behavior shown for the fast flux in Fig. 11. This is due to the alternating arrangement of fuel zones and moderating regions (the side plates, the central flux trap, and the water-filled control channels). In the fuel regions the fast flux is high and the thermal flux is low, and just the opposite occurs in the moderating regions.

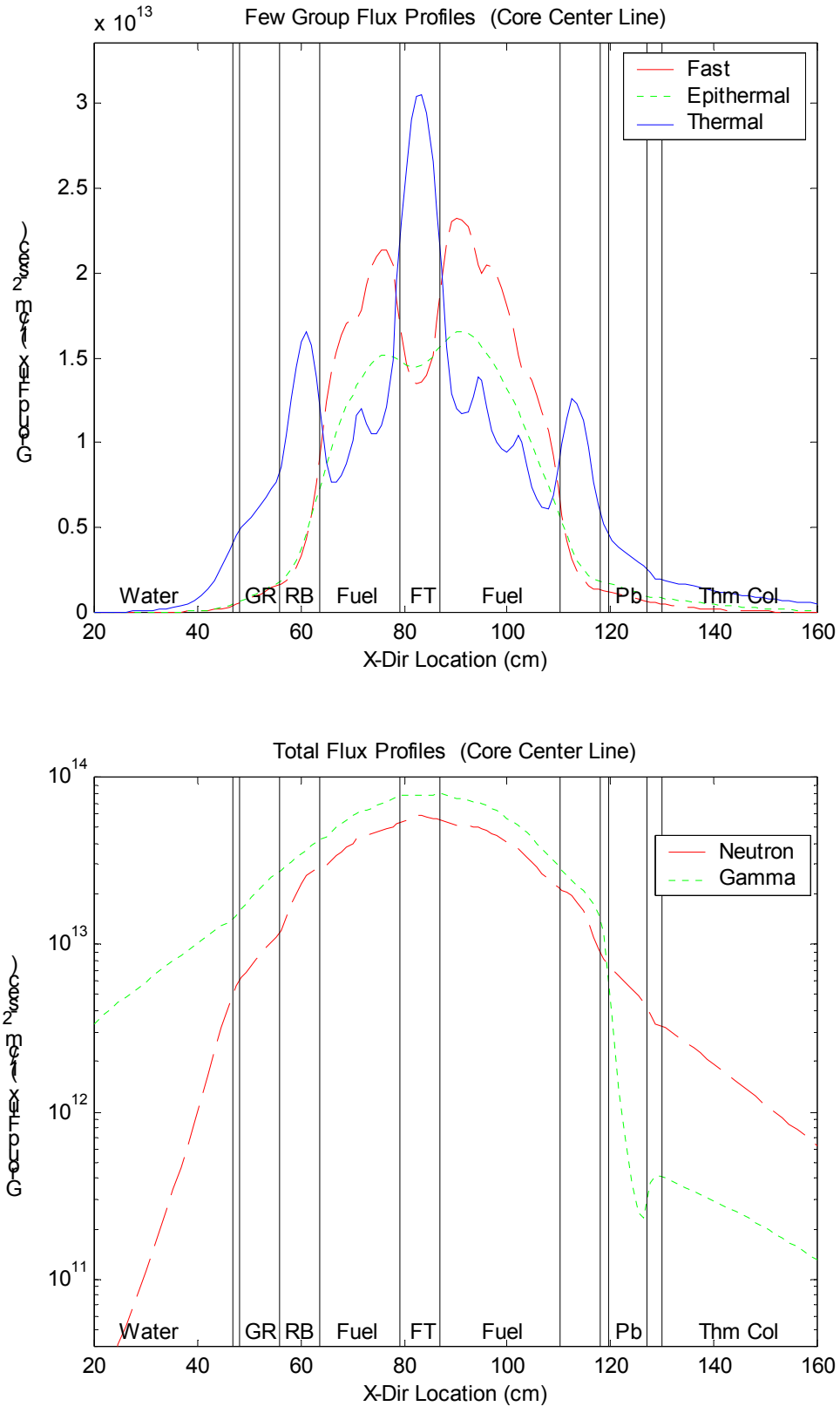

Fig. 10 Typical X-directed flux profiles along the core centerline.

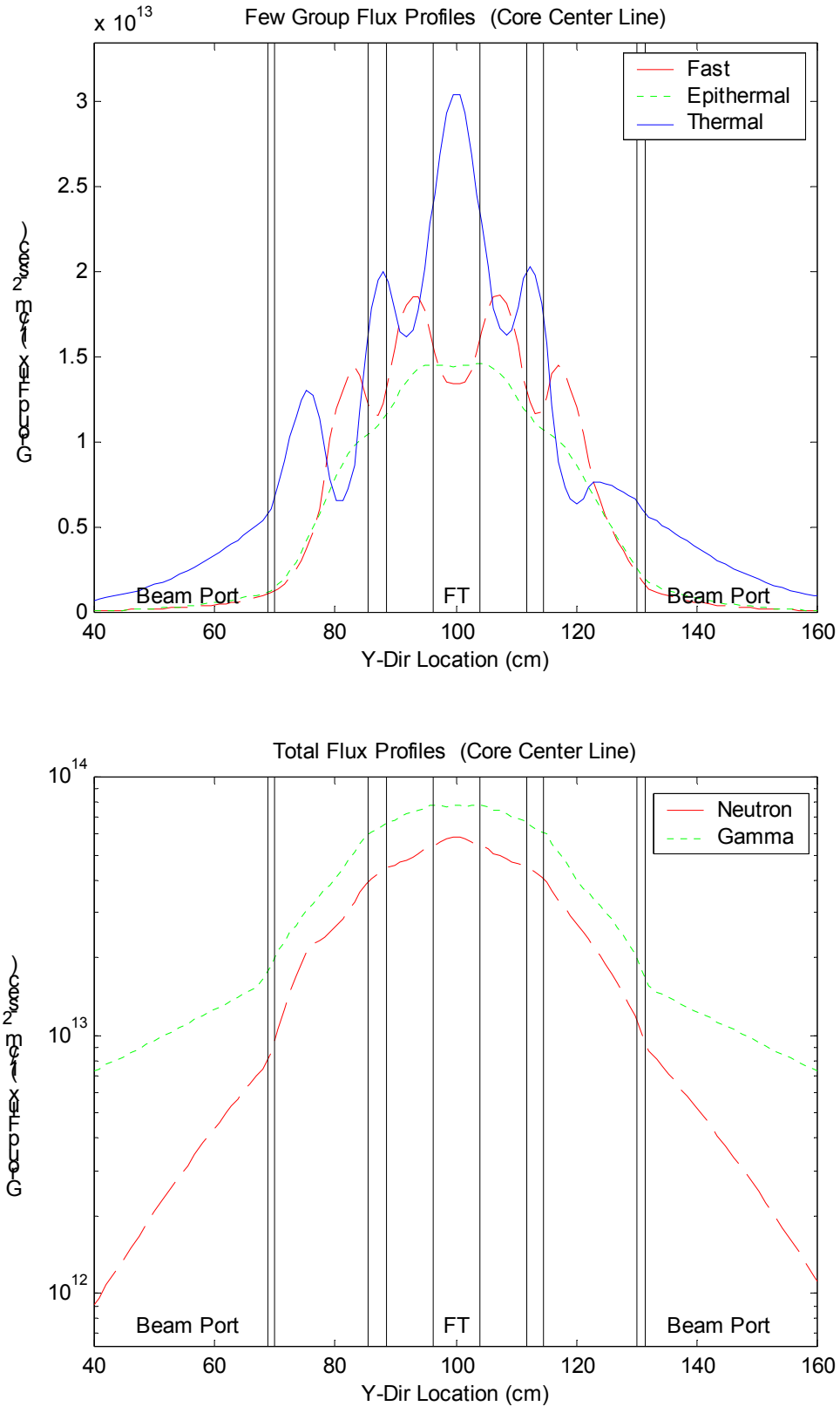

Fig. 11 Typical Y-directed flux profiles along the core centerline.

Spectral Distributions (E-profiles)

The 67-group DORT fluxes in several irradiation regions were averaged over the spatial zone of interest and separated into a neutron flux vector (47 groups) and a gamma flux vector (20 groups). These data for the radiation basket in D2, the flux trap in D5, and two beam port edit regions near the core box are plotted versus energy in Figs. 12 and 13 -- the neutron spectra are in Fig. 12 and the gamma spectra are shown in Fig. 13. These two figures illustrate the general magnitude and spectral characteristics expected within the key experimental facilities in the UMLRR, and they are quite typical of water-cooled thermal systems. The individual neutron and gamma spectral distributions are qualitatively similar (on a log scale) but, of course, the magnitudes vary by zone. These data are of particular interest to researchers using a specific irradiation facility for their experiments.

Integral Results for the Irradiation Facilities

One often would like to have a single number to characterize the flux spectrum in a given location and energy region. This information can be approximated from the space and energy profiles just discussed but, because the variation is so rapid in some regions, this approach is very approximate at best. However, the post-processing steps mentioned above also perform integrals over energy and space as desired (defined via user input). In particular, the zone-average values for the broad-group fluxes and other responses for several irradiation zones were extracted from the code output and they are summarized in Table I. The data are broken into three broad categories -- broad-group fluxes, additional characterization of the fast flux component of the spectrum, and information concerning energy deposition rates in the various facilities.

The broad-group neutron flux data are tabulated as fast, epithermal, and thermal fluxes with the same energy bins as described above. Also included are entries for the total neutron and gamma particle flux in the particular zone of interest. These data from Table I can be correlated directly to the information given in Figs. 10-13. Also tabulated are estimates of the average fluxes that would be observed if the experimental bayonets were inserted into the radiation basket in D2 and the flux trap in D5 (this was done in a single perturbation calculation). As apparent, a sizable perturbation relative to the experiment-free fast and thermal fluxes near the irradiation locations is observed. This is highlighted even further in Fig. 14, where we compare the X-directed flux profiles for the cases with and without the bayonet present. In this case, the air-filled bayonet displaces some of the water in the irradiation zone, which results in a higher fast flux and a lower thermal flux near the perturbation. This illustration is important since it emphasizes that the insertion of experiments into the UMLRR can cause fairly large local flux perturbations -- and most of the results given here are for the reference experiment-free configuration.

Additional characterization of the fast component of the spectrum is important because many of the material irradiations performed in the UMLRR focus on fast neutron studies. Many researchers are interested in the neutron fluence above 1 MeV, while others include all neutrons above 0.01 MeV (plus we have already tabulated the > 0.1 MeV flux as group 1 of the 3-group structure). In addition, because of the historical use of the facility for irradiation of electronic components, it is also important to quantify the so-called 1 MeV equivalent flux for silicon displacement in the various experimental locations of the UMLRR.

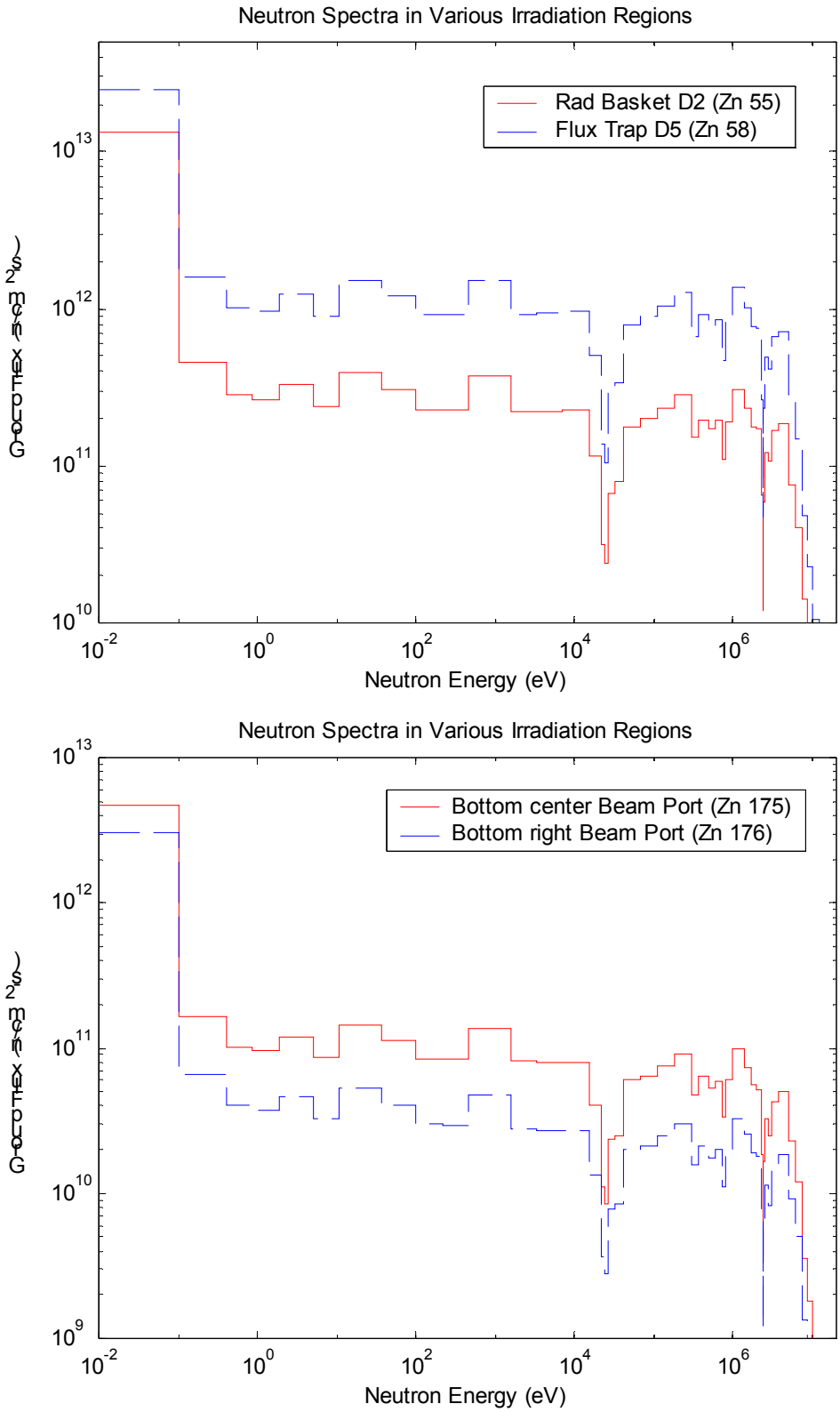

Fig. 12 Neutron flux spectra in various irradiation facilities.

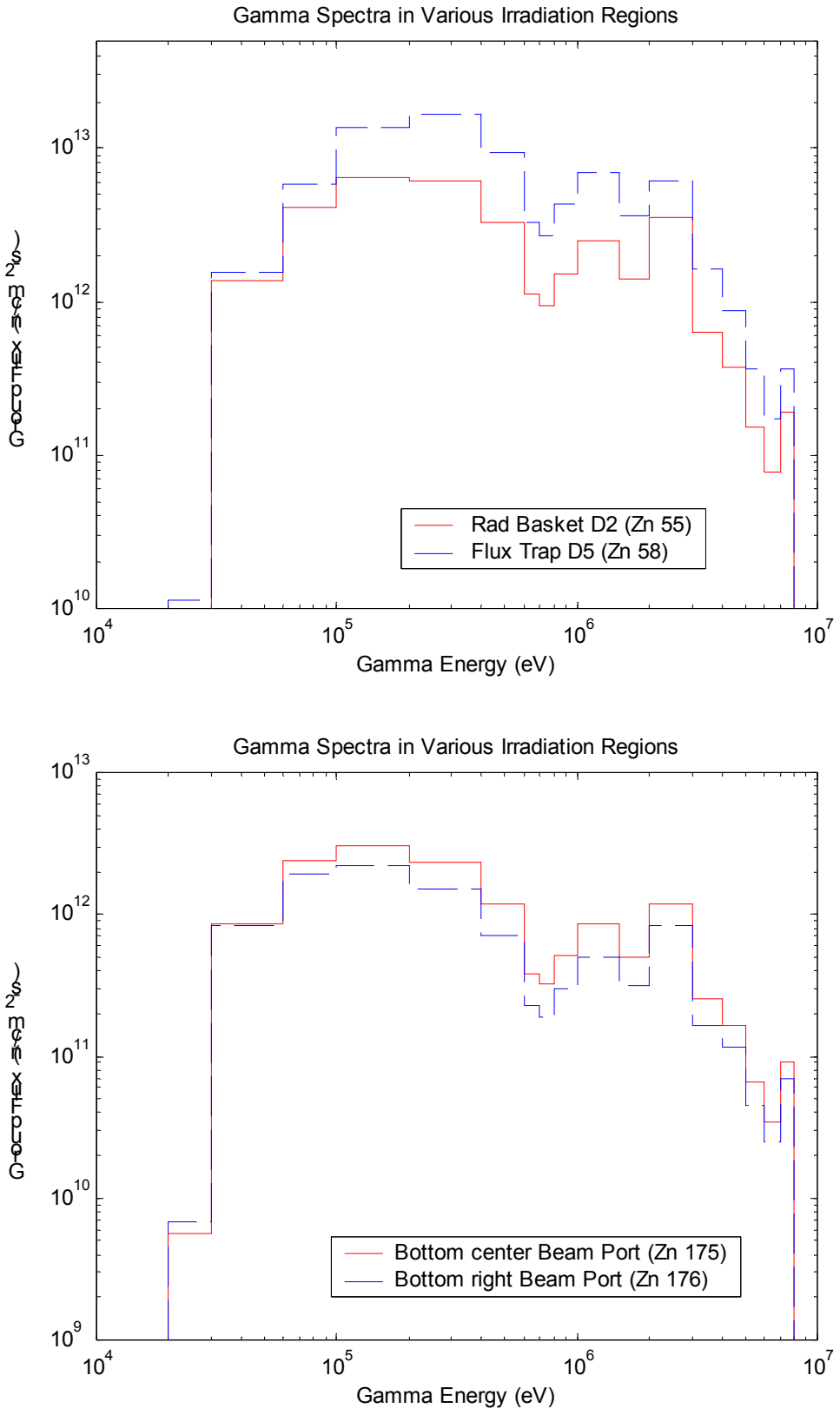

Fig. 13 Gamma flux spectra in various irradiation facilities.

Table I Average flux data and other responses for several irradiation regions in the reference LEU core.

Irradiation Region →	Radiation Basket (D2) (Zone 55)		Flux Trap (D5) (Zone 58)		Center Beamport (Zone 175)	Right Beamport (Zone 176)	Thermal Column (Zone 177)	Thermal Column (Zone 178)
Parameter of Interest	**no bayonet**	**with bayonet**	**no bayonet**	**with bayonet**	**no bayonet**	**no bayonet**	**no bayonet**	**no bayonet**
Broad Group Fluxes (n/cm^2-sec)								
Fast Flux (> 0.1 MeV)	3.33E+12	3.78E+12	1.43E+13	1.63E+13	1.01E+12	3.44E+11	2.68E+11	7.10E+10
Epithermal Flux	3.64E+12	4.07E+12	1.47E+13	1.55E+13	1.31E+12	4.65E+11	5.99E+11	2.58E+11
Thermal Flux (<1 eV)	1.41E+13	1.35E+13	2.74E+13	2.09E+13	5.00E+12	3.17E+12	1.54E+12	9.05E+11
Total Neutron Flux	2.10E+13	2.14E+13	5.64E+13	5.27E+13	7.32E+12	3.98E+12	2.40E+12	1.23E+12
Total Gamma Flux	3.39E+13	3.35E+13	7.75E+13	7.50E+13	1.41E+13	9.97E+12	3.33E+11	2.20E+11
Additional Fast Flux Characterization								
Fast Flux (> 1 MeV)	1.75E+12	1.97E+12	7.27E+12	8.15E+12	5.11E+11	1.79E+11	8.75E+10	2.17E+10
Fast Flux (> 0.01 MeV)	4.12E+12	4.67E+12	1.78E+13	2.01E+13	1.28E+12	4.33E+11	4.07E+11	1.22E+11
1 MeV Equivalent Flux	3.13E+12	3.53E+12	1.32E+13	1.49E+13	9.34E+11	3.22E+11	2.11E+11	5.49E+10
RDF	0.76	0.76	0.74	0.74	0.73	0.74	0.52	0.45
Energy Deposition Rate (rad/hr)								
Neutrons in Air	3.09E+07	3.03E+07	6.81E+07	5.74E+07	1.07E+07	6.51E+06	3.14E+06	1.79E+06
Neutrons in Water	3.27E+07	3.69E+07	1.37E+08	1.55E+08	9.71E+06	3.36E+06	2.19E+06	5.84E+05
Gammas in Air	3.84E+07	3.84E+07	9.04E+07	8.86E+07	1.42E+07	9.38E+06	4.39E+05	1.94E+05
Gammas in Water	4.26E+07	4.26E+07	1.00E+08	9.83E+07	1.57E+07	1.04E+07	4.85E+05	2.16E+05

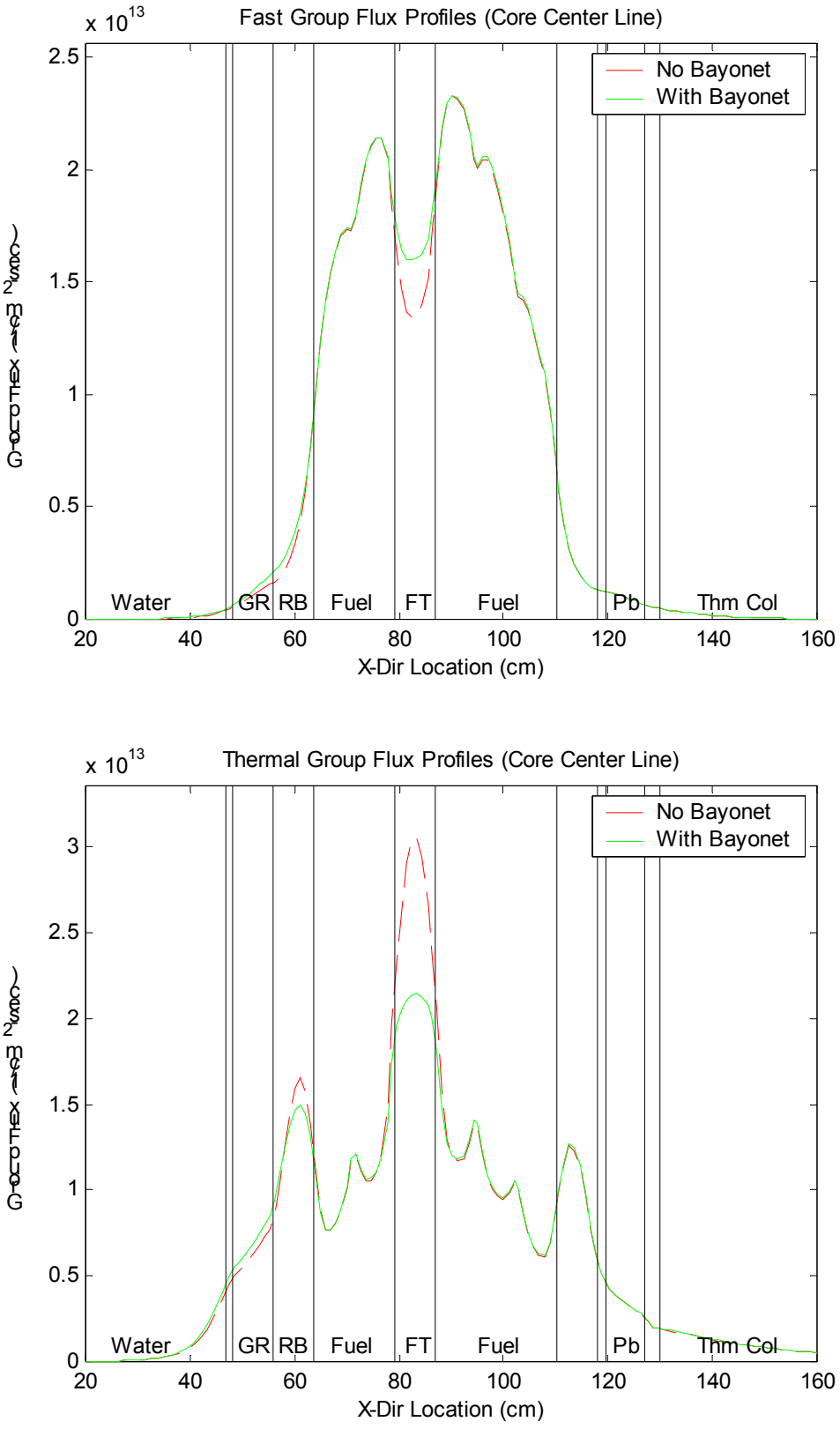

Fig. 14 Effect of the experimental bayonet on the local flux distribution.

The 1 MeV equivalent flux for silicon displacement is formally defined[9] as

$$\phi_{eq}(E_o) = \frac{\int_{E_{min}}^{E_{max}} K_D(E)\phi(E)dE}{K_D(E_o)} \tag{7}$$

where $K_D(E)$ is the neutron displacement kerma for silicon as a function of energy, E_o is the reference energy of interest, and E_{min} and E_{max} specify the energy range for significant atomic displacement in silicon. Reference 9 suggests the use of 0.01 MeV and 18 MeV as limits for the energy range of interest and E_o is usually 1 MeV. The suggested value for the displacement kerma at 1 MeV is 95,000 eV-b, and this is used as $K_D(E_o)$ in eqn. (7).[9] The energy-dependent kermas used in this study were obtained from the BUGLE-96 library,[8] since the 47-group energy structure in BUGLE-96 is identical to the energy bins chosen for this study.

Reference 9 also defines the "neutron energy spectrum hardness parameter" or simply the relative damage factor (RDF). The RDF is given by

$$RDF = \frac{\int_{E_{min}}^{E_{max}} K_D(E)\phi(E)dE}{K_D(E_o)\int_{E_{min}}^{E_{max}} \phi(E)dE} = \frac{\phi_{eq}(E_o)}{\phi_T} \tag{8}$$

where ϕ_T is the total energy-integrated flux over the interval of interest. The RDF is a convenient measure for characterizing the spectrum of a particular facility. It represents the fluence of 1 MeV neutrons required to produce the same displacement kerma in silicon as a unit fluence of neutrons of spectral distribution $\phi(E)$.

The relative damage factor (RDF) and the other fast flux characterization parameters are given in the second part of Table I. As expected, the flux trap has the largest fast fluence, with some fast flux values above $1x10^{13}$ n/cm^2-sec. However, the RDF for the beamports, radiation baskets, and flux trap are all in a narrow range of 0.73 - 0.76. This indicates that the fast spectra above 0.01 MeV in these regions are very similar. Also, as expected, the RDF in the two thermal column edit zones is significantly lower, indicating a much softer flux spectrum in this particular irradiation facility.

Finally, Table I also gives some data concerning energy deposition in air and in water for the different UMLRR irradiation facilities. The kerma factors used to compute these dose rates are directly from the BUGLE-96 library.[8] These data are useful as a qualitative indication of the expected dose rates in the various facilities. For a particular experiment, material-specific kermas would be needed to estimate actual energy deposition within the specific sample. The dose rate data in the bottom part of Table I are still useful, however, because they give a good indication of the relative neutron and gamma dose rates and how these vary for the different experimental facilities.

FUTURE WORK

The data generated as part of this project have helped characterize the radiation environments that are expected within several of the experimental facilities in the proposed UMLRR LEU

core. Certainly the computational models have inherent limitations, but the results generated here should paint a reasonably accurate picture of expected behavior within the new LEU core. However, definitive validation of the model predictions is nearly impossible until direct comparisons to measured data are made. Thus, our studies will not be 100% complete until rigorous comparisons of our model prediction capability and the measured data from the operating facility are performed. Hopefully this will take place during the summer of 2000 when the new LEU core is operational and experimental data begin to become available.

ACKNOWLEDGEMENTS

This work was supported by a Department of Energy grant under Project #14-08239-F through the University of Massachusetts Lowell Research Foundation.

REFERENCES

1. J. R. White and R. D. Tooker, "Modeling and Reference Core Calculations for the LEU-Fueled UMass-Lowell Research Reactor," ANS 1999 Winter Meeting, Long Beach, CA (Nov. 1999).
2. "VENTURE-PC - A Reactor Analysis Code System," Radiation Safety Information Computational Center, CCC-654 (1997).
3. "DOORS3.1 - One, Two, and Three Dimensional Discrete Ordinates Neutron/Photon Transport Code System," Radiation Safety Information Computational Center, CCC-650 (1996).
4. "MCNP-4B - Monte Carlo N-Particle Transport Code System," Radiation Safety Information Computational Center, CCC-660 (1997).
5. J. R. White, et. al., "Calculational Support for the Startup of the LEU-Fueled UMass-Lowell Research Reactor," Topical Meeting on Advances in Reactor Physics and Mathematics and Computation (these proceedings), Pittsburgh, PA (May 2000).
6. "SCALE 4.3 - Modular Code System for Performing Standardized Computer Analyses for Licensing Evaluation for Workstations and Personal Computers," Radiation Safety Information Computational Center, CCC-545 (1997).
7. "VITAMIN-B6 - A Fine-Group Cross Section Library Based on ENDF/B-VI Release 3 for Radiation Transport Applications," Radiation Safety Information Computational Center, DLC-184 (1996).
8. "BUGLE-96 - Coupled 47 Neutron, 20 Gamma-Ray Group Cross Section Library from ENDF/B-VI for LWR Shielding and Pressure Vessel Dosimetry Applications," Radiation Safety Information Computational Center, DLC-185 (1996).
9. "Characterizing Neutron Energy Fluence Spectra in Terms of an Equivalent Monoenergetic Neutron Fluence for Radiation-Hardness Testing of Electronics," ASTM Standard Practice E722-85 (1985).